Inorganic Chemistry

Article

pubs.acs.org/IC

Understanding the Crystallization Mechanism of Delafossite $CuGaO_2$ for Controlled Hydrothermal Synthesis of Nanoparticles and Nanoplates

Mingzhe Yu, Thomas I. Draskovic, and Yiying Wu*

Department of Chemistry and Biochemistry, The Ohio State University, 100 West 18th Avenue, Columbus, Ohio 43210, United States

Supporting Information

ABSTRACT: The delafossite $CuGaO_2$ is an important p-type transparent conducting oxide for both fundamental science and industrial applications. An emerging application is for p-type dye-sensitized solar cells. Obtaining delafossite $CuGaO_2$ nanoparticles is challenging but desirable for efficient dye loading. In this work, the phase formation and crystal growth mechanism of delafossite $CuGaO_2$ under low-temperature (<250 °C) hydrothermal conditions are systematically studied. The stabilization of Cu^I cations in aqueous solution and the controlling of the hydrolysis of Ga^{III} species are two crucial factors that determine the phase formation. The oriented attachment (OA) growth is proposed as the crystal growth mechanism to explain the formation of large $CuGaO_2$ nanoplates. Importantly, by suppressing this OA process, delafossite $CuGaO_2$ nanoparticles that are 20 nm in size were successfully synthesized for the first time. Moreover, considering the structural and chemical similarities between the Cu-based delafossite series compounds, the understanding of the hydrothermal chemistry and crystallization mechanism of $CuGaO_2$ should also benefit syntheses of other similar delafossites such as $CuAlO_2$ and $CuScO_2$.

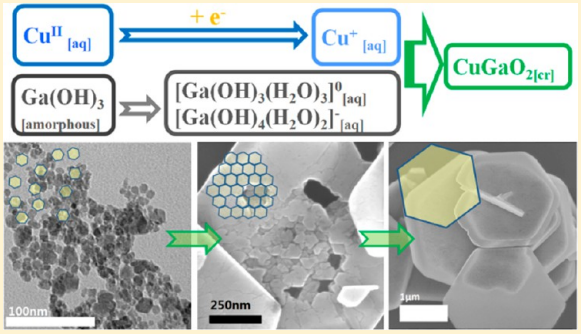

INTRODUCTION

Delafossite $CuGaO_2$ is an interesting p-type transparent conducting oxide.[1,2] It has a layered structure with alternating linearly coordinated O−Cu^I−O layers and edge-sharing octahedral GaO_6 layers. By adopting the ABCABC or ABABAB stacking, the crystal can have either a rhombohedra (3*R*) or hexagonal (2*H*) symmetry (Figure 1). The physicochemical properties of delafossite $CuGaO_2$ have been investigated via both theoretical and experimental approaches: the valence band (VB) edge, which locates at ∼5.1 eV below vacuum level, is a hybrid of the Cu 3*d* orbital and O 2*p* orbital and is therefore delocalized from the oxygen atoms.[3−5] With the holes induced by Cu vacancy and O interstitial defects, the material is p-type conductive with a carrier mobility reported as $\sim 10^{1}-10^{-2}$ cm^2 V^{-1} s^{-1}.[3−5] In the lattice of delafossite $CuGaO_2$, the Cu^I has a close-shelled d^{10} configuration, and the Cu to Cu coupling is two-dimensional. Hence the coloration factors, which may reduce the bandgap, are weak. As a result, the material has a large optical bandgap E_g, with values in the range of 3.4−3.7 eV.[6,7] With its excellent p-type conductivity and high transparency, the delafossite $CuGaO_2$ holds great promise in multiple applications such as p−n junction transparent electronics, p-type dye-sensitized solar cells (p-DSCs), photo and chemical catalysis, etc.[8−17]

Among the different applications, the delafossite $CuGaO_2$ is especially attractive for p-DSCs. With a lower VB edge, larger optical bandgap, and higher conductivity, $CuGaO_2$ is a promising alternative p-type semiconductor to the commonly used NiO.[11,12,14,15,17] The $CuGaO_2$-based p-DSCs have shown higher open-circuit voltages and better charge transport than the NiO-based ones. However, because of the large particle size of $CuGaO_2$, the photocurrent density is limited. For p-DSCs, nanoparticles are desirable for efficient dye loading. Therefore, developing synthetic methods of delafossites with controlled sizes is important for achieving their potential.

Conventional syntheses of delafossite $CuGaO_2$ include solid-state reactions[6,18−20] and vacuum-deposition techniques.[7,19,21] Both methods have their limitations: the solid-state synthesis yields large and agglomerated particles (typical size >1 μm) due to the high-temperature sintering, while vacuum-deposition techniques require demanding experimental conditions and are not applicable for obtaining nanostructures. The recently developed hydrothermal method has provided chances to synthesize delafossite $CuGaO_2$ at a relatively low temperature, which is more convenient and cost-efficient.[22−26] Poeppelmeier and co-workers pioneered the "Teflon-pouch method" to synthesize a series of Cu- and Ag-based delafossite compounds at low temperature (<210 °C) hydrothermal conditions.[24,25] In their study, binary metal oxides were used as precursors, and sodium hydroxide was used as a mineralizer. The authors pointed out that the acid−base character of a constituent oxide

Received: March 31, 2014
Published: May 15, 2014

   dx.doi.org/10.1021/ic500747x | *Inorg. Chem.* 2014, 53, 5845−5851

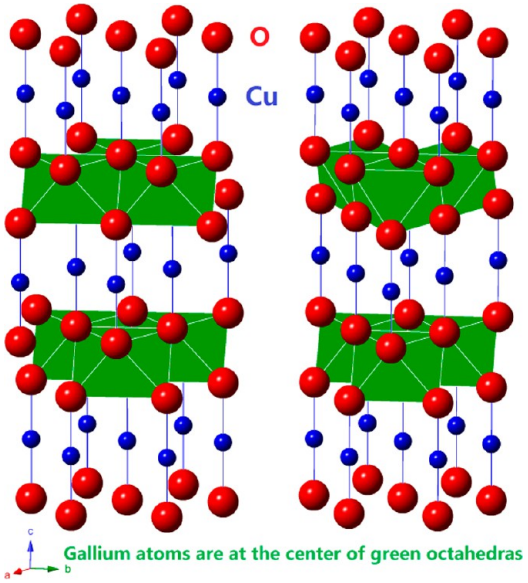

Figure 1. The crystal structure of the delafossite $CuGaO_2$. (left) Rhombohedra (3*R*). (right) Hexagonal (2*H*). (Axes based on the hexagonal 2*H* symmetry).

determines its solubility in solvents and therefore affects the phase formation of corresponding delafossite products. Their synthesized $CuGaO_2$ particles were on the micrometer scale. More recently, Cario and co-workers reported the hydrothermal synthesis of $CuGaO_2$, starting with soluble metal nitrate salts as precursors and ethylene glycol as a reducing agent for obtaining Cu^I.[23,26] By tuning the pH of the precursor, $CuGaO_2$ nanoplates with size varying from ~1 μm to ~300 nm were synthesized. However, further reduction of the particle size is still needed, which requires greater understanding of the crystallization process.

In this work, we systematically studied the phase formation and particle growth mechanism of delafossite $CuGaO_2$ under hydrothermal conditions with soluble metal salts as precursors. The stabilization of Cu^I cations in aqueous solvent and the control of the hydrolysis of Ga^{III} species are two key factors that determine the $CuGaO_2$ phase formation. By monitoring the product morphologies at the early stage of reactions, we propose the oriented attachment (OA) growth as the crystal growth mechanism. By suppressing the OA growth, delafossite $CuGaO_2$ with a 20 nm size was successfully synthesized for the first time. On the other hand, large $CuGaO_2$ nanoplates (>1 μm in diameter) were also synthesized with the OA growth promoted. The controlled synthesis will be of interest to the applications of $CuGaO_2$ in p-DSCs and transparent electronics. Moreover, since Cu-based delafossite compounds share the structural and chemical similarities, the knowledge gained of the crystallization mechanism of $CuGaO_2$ should also benefit future research on other similar compounds such as $CuAlO_2$ and $CuScO_2$.

RESULTS AND DISCUSSION

The Hydrothermal Chemistry and Phase Formation of Delafossite $CuGaO_2$. To trigger the phase formation of $CuGaO_2$, the coexistence of proper Cu^I and Ga^{III} aqueous species in the hydrothermal system is required. The first challenge is to control the oxidation state of Cu to be +1 in the solution. With the addition of reducing reagents to the precursor, the Cu^{II} can be reduced to Cu^I. However, according to the Pourbaix diagram of copper,[27] $Cu^I_{[aq]}$ is not stable at room temperature, easily disproportionating into Cu^0 and Cu^{II}, or it precipitates out as $Cu_2O_{[cr]}$. The stable "window" for $Cu^I_{[aq]}$ appears as temperature increases. At 200 °C, the dominant aqueous species of copper is $Cu^+_{[aq]}$ when pH < ~6.8 and $Cu^I(OH)_{[aq]}$ when ~7 < pH < ~8.8. Both $Cu^+_{[aq]}$ and $Cu^I(OH)_{[aq]}$ have the desired oxidation state. However, due to its low solubility (i.e., $\sim 10^{-3}$–10^{-4} mM), $Cu^I(OH)_{[aq]}$ will easily precipitate out as $Cu_2O_{[cr]}$.[27,28] Therefore, we only consider $Cu^+_{[aq]}$, which can be stabilized at pH < 6.8 and a high temperature (ca. ~200 °C), as the proper Cu species.

Then we consider the hydrolysis and condensation of Ga^{III} species. In aqueous solution, the degree of hydrolysis and hydrolyzed species are predominantly determined by the solution pH. According to the Ga^{III} speciation distribution diagram[29] at 250 °C, the dominant Ga^{III} aqueous species is $[Ga(OH)_2(H_2O)_4]^+$ when pH < ~ 3; then it turns to $[Ga(OH)_3(H_2O)_3]^0$ when ~3 < pH < ~ 4.3 and $[Ga(OH)_4(H_2O)_2]^-$ (*or* $Ga(OH)_4^-$) when pH > ~ 4.3. Since the positively charged $Cu^+_{[aq]}$ is participating in the $CuGaO_2$ phase formation, the negatively charged $[Ga(OH)_4(H_2O)_2]^-_{[aq]}$ or neutral $[Ga(OH)_3(H_2O)_3]^0_{[aq]}$ should be more favored to proceed through the nucleophilic reaction with $Cu^+_{[aq]}$. Therefore, a pH > 3 should be selected to avoid the existence of $[Ga(OH)_2(H_2O)_4]^+_{[aq]}$. The proposed phase formation process is shown in the following reaction equations:

$$Cu^+_{[aq]} + [Ga(OH)_4(H_2O)_2]^-_{[aq]} \rightarrow CuGaO_{2[cr]} + 4H_2O \quad (1)$$

$$Cu^+_{[aq]} + [Ga(OH)_3(H_2O)_3]^0_{[aq]} \rightarrow CuGaO_{2[cr]} + 3H_2O + H_3O^+ \quad (2)$$

One competing process to the $CuGaO_2$ formation is the self-condensation of Ga^{III} species into crystallized γ-GaO(OH):

$$Ga(OH)_{3[amorphous]} \rightarrow \gamma\text{-}GaO(OH)_{[cr]} + H_2O \quad (3)$$

$$[Ga(OH)_3(H_2O)_3]^0_{[aq]} \rightarrow \gamma\text{-}GaO(OH)_{[cr]} + 4H_2O \quad (4)$$

Under hydrothermal conditions, the γ-GaO(OH) crystal is kinetically stable once formed.[30] Therefore, we should not perform the synthesis at pH ≈ 3.2, where $GaO(OH)_{[aq]}$ reaches its lowest solubility (ca. 10^{-3}–10^{-4} mM at 200 °C).[29]

On the basis of the above analysis, the hydrothermal synthetic process is summarized in Scheme 1: first, copper and gallium nitrate are dissolved in water with pH tuned by potassium hydroxide, forming a soluble precursor. The ethylene glycol (or other alcohols) is added as reducing reagent.[23,31]

Scheme 1. The Proposed Phase Formation of Delafossite $CuGaO_2$ in the Hydrothermal Synthesis

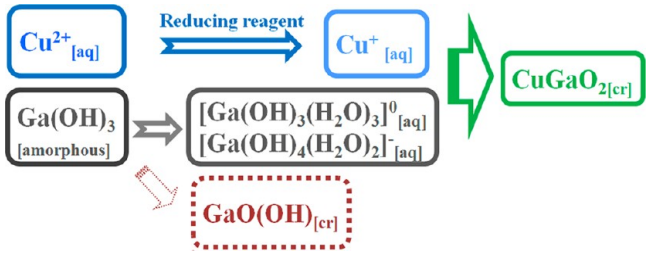

dx.doi.org/10.1021/ic500747x | Inorg. Chem. 2014, 53, 5845–5851

Upon hydrothermal heating, $Cu^{2+}_{[aq]}$ is reduced to $Cu^{+}_{[aq]}$ and stabilized. It then reacts with $[Ga(OH)_4(H_2O)_2]^-_{[aq]}$ and $[Ga(OH)_3(H_2O)_3]^0_{[aq]}$ species to form the delafossite $CuGaO_2$. Meanwhile, the hydrolyzed Ga^{III} species can also possibly form γ-$GaO(OH)_{[cr]}$ through a self-condensation process. The appropriate synthetic conditions for forming delafossite $CuGaO_2$ is predicted to be at a high temperature (ca. ~200 °C or higher) and a pH in between ~3 and ~6.5, with the presence of reducing reagent.

According to the proposed mechanism, the reaction temperature and pH of the precursor are two crucial parameters that determine the $CuGaO_2$ formation. To verify the effects of reaction temperature, a series of reactions were performed at different temperatures (with other parameters kept the same; see Experimental Section for details). Figure 2 shows the

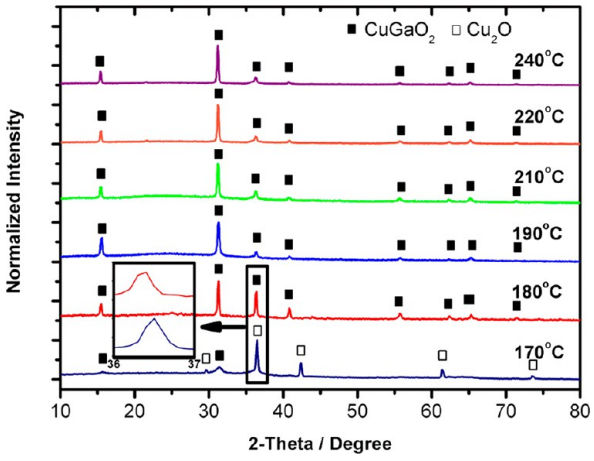

Figure 2. The XRD patterns of products synthesized with variable temperatures.

powder X-ray diffraction (XRD) patterns of the products obtained at different reaction temperatures. At pH ≈ 5.2, the delafossite $CuGaO_2$ 3*R* phase (the International Centre for Diffraction Data powder diffraction file: ICDD-PDF#41−0255) was detected in all reactions when the temperature was higher than 180 °C. While at 170 °C (and lower), the main product was Cu_2O. Similarly, to check the pH effect, another series of reactions were performed at 190 °C with the precursor pH tuned from ~2.3 to ~11.3. According to XRD results (Figure 3), the delafossite 3*R* $CuGaO_2$ was formed as the main product in the pH range from ~3.4 to ~6.6. When the pH was lower than ~3.4, γ-GaO(OH) was observed; Cu_2O, Cu, and CuO were produced if the pH was higher than ~7.7. The experimental results agree well with our prediction: a high temperature and a proper pH window are needed for the stabilization of Cu^{I} and the negatively charged or neutral Ga^{III} species in the solution for the $CuGaO_2$ formation.

Regarding the proposed mechanism, to clarify whether γ-GaO(OH) is participating in the formation of $CuGaO_2$ as an intermediate product, γ-GaO(OH) powder was used in the precursor to replace gallium nitrate for the reaction. The XRD pattern (Figure 4) shows the dominant product after the hydrothermal reaction was still γ-GaO(OH), with no detectable $CuGaO_2$ peaks. This confirms our prediction that the γ-GaO(OH) is kinetically stable once formed and not participating in the $CuGaO_2$ formation. It is also worth mentioning that besides ethylene glycol, other soluble alcohols, including methanol, ethanol, and isoproponal, were tried as

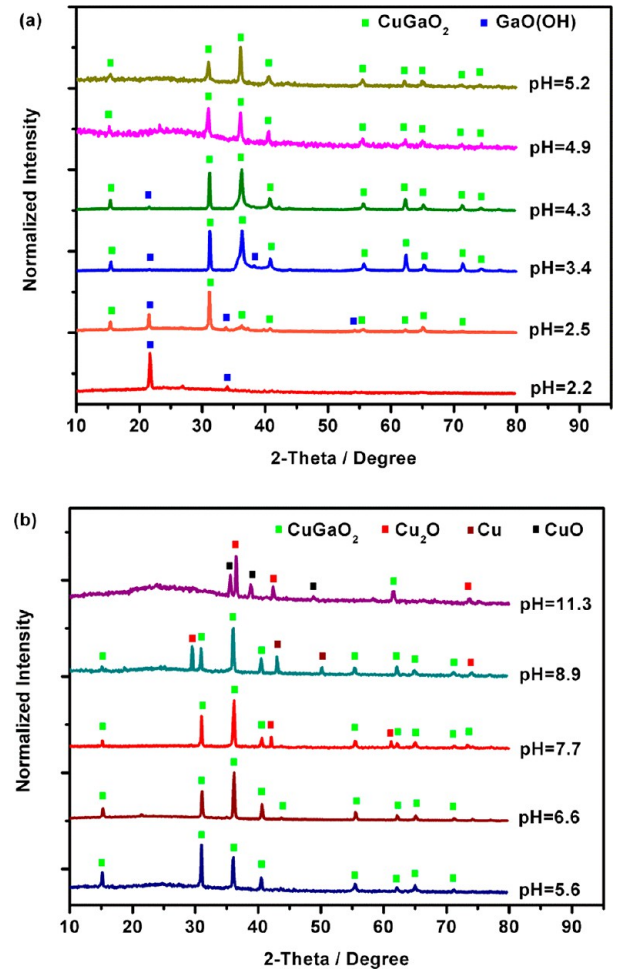

Figure 3. The XRD patterns of products synthesized with variable pH values. (a) pH = 2.2 to 5.2. (b) pH = 5.6 to 11.3.

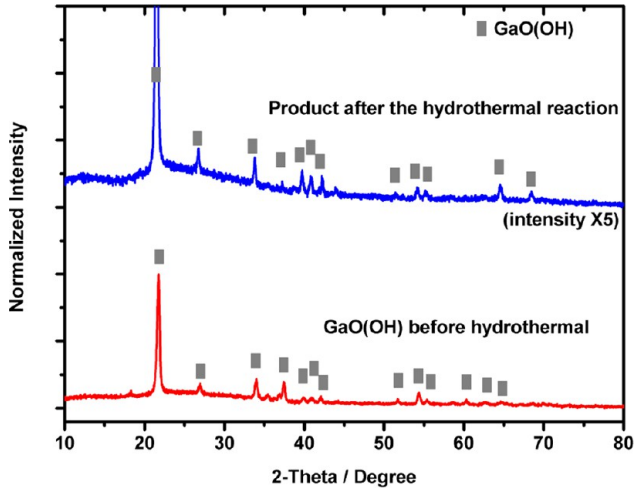

Figure 4. XRD pattern of the products from the reaction with GaO(OH) as precursors.

reducing reagents in the synthesis, and the $CuGaO_2$ was produced as well. However, neither ketones nor amines worked, probably because the reducing capability is too weak for the former one while too strong for the latter one (see Supporting Information, Figure S1).

dx.doi.org/10.1021/ic500747x | Inorg. Chem. 2014, 53, 5845−5851

Oriented Attachment (OA) Growth of Delafossite $CuGaO_2$ Nanocrystals. After probing the hydrothermal chemistry for the $CuGaO_2$ phase formation, now we focus on the crystal growth mechanism. There are two types of crystal growth modes: one is the classical Ostwald ripening,[32] which is via the atom-by-atom additions to an existing nucleus or the dissolution of unstable phases and reprecipitation of more stable phases. The second one, the oriented attachment (OA) growth, has been proposed as an equally significant process for crystal growth.[33,34] During the OA growth, primary nanocrystals are first formed and act as building blocks for the secondary monocrystalline nanostructures.[33,35,36] In the suspension, primary nanocrystals continuously undergo rotation and interaction until they are aligned with a perfect lattice match. The coalescence of neighboring particles then happens by eliminating a common boundary, and a larger secondary structure is produced. Meanwhile, the surface reconstruction of the secondary structure leads to the formation of large monocrystalline particles.[37−39] Interactions between primary nanocrystals include attractive forces, which are mainly the van der Waals force, and repulsive forces, including electrostactic and steric repulsions. The van der Waals attraction favors the alignment of primary nanocrytals and OA growth, while the electrostatic and steric repulsions tend to keep primary nanocrystals away from each other and inhibit OA growth.

In the synthesis, by collecting the products formed at the early stage of growth, we successfully captured the particles in the "intermediate state." From scanning electron microscopy (SEM) and high-resolution transmission electron microscopy (HRTEM) images, we are able to identify the attachment of small particles at the edge of large plates, the void in the plates, and the rough basal surfaces composed of attached smaller particles (Figure 5). On the basis of these observations, we propose the OA process as the $CuGaO_2$ crystal growth mechanism: primary delafossite $CuGaO_2$ nanocrystals are first formed in the solution at the beginning of the reaction and then go through the OA growth, growing into large nanoplates (Scheme 2). Because of its highly anisotropic crystal structure (Figure 1), the surface charge density of the basal plane of delafossite $CuGaO_2$ particles is significantly higher than that of others. A higher surface charge density provides stronger repulsive forces, suppressing the OA growth along this direction; therefore, crystals with a plate-like morphology are more preferred in the final product.

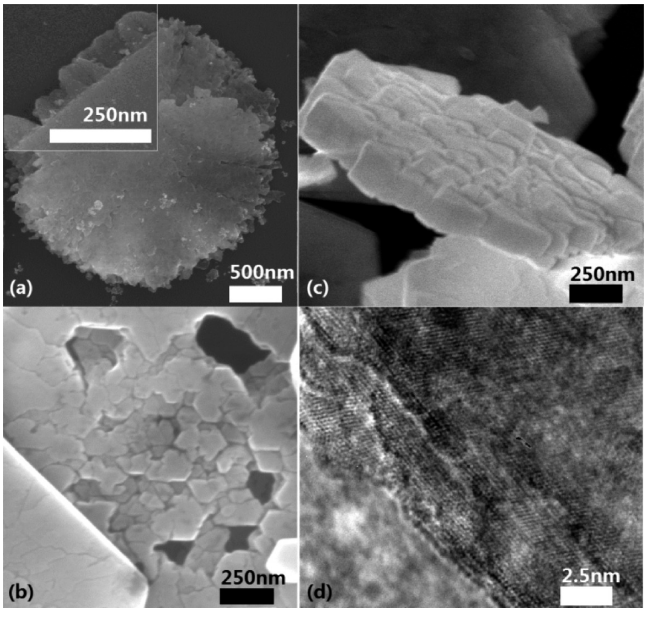

Figure 5. SEM and HRTEM images of the $CuGaO_2$ nanoplates. (a) The edge shows the size of new nanocrystals attached. (b, c) A closer view of the basal surfaces showing the large plates are made of smaller nanocrystals, which result in the rough surfaces. (d) The HRTEM shows the rough edges of the nanoplates.

As discussed above, a stronger repulsion inhibits the OA process, yielding smaller particles in final products; a weaker repulsion promotes the OA process, and larger nanoplates are expected to form. By tuning synthetic parameters, including the pH of precursor, the reaction temperature, the addition of surfactants, the concentration of the precursor, and the reaction time, we are able to adjust the electrostatic and steric repulsions and thereby achieve control of the final product morphology.

The pH of the Precursor Solution. We first measured the isoelectric point (IEP) of $CuGaO_2$ nanoparticles to be ∼6.7 in aqueous solutions (Supporting Information, Figure S2). This means that, when the precursor pH is closer to 6.7, less surface charge will remain on the primary nanoparticles. The weak electrostatic repulsion between nanoparticles promotes the OA process. With the solution pH farther from 6.7, the OA growth will be inhibited due to the stronger electrostatic repulsions.

The Reaction Temperature. The electrostatic repulsion force is inversely proportional to the dielectric constant of the aqueous medium. The dielectric constant of water decreases as the temperature increases.[40] Therefore, a higher reaction temperature would suppress the OA growth of $CuGaO_2$, while a lower reaction temperature would favor this process.

The Addition of Surfactants. By binding on particle surfaces, the surfactant molecules create a barrier for nanoparticles to approach each other and induce a strong steric repulsion. In the $CuGaO_2$ synthesis, the addition of an appropriate amount of surfactants will efficiently prevent the newly formed $CuGaO_2$ nanocrystals from growing into large nanoplates. As an example, we added sodium dodecyl sulfate (SDS, 1:1 ratio vs copper ion concentration) as the surfactant and observed the formation of small nanoparticles with ∼20 nm size (Supporting Information, Figure S3).

The Concentration of the Precursor. The rate of OA growth depends on the effective collision frequency of primary nanoparticles. The concentration of the precursor controls the concentration of formed primary nanocrystals. Therefore, a higher precursor concentration would accelerate the OA process. Within the same reaction time, a higher precursor concentration is preferred for large nanoplates, while a lower precursor concentration is preferred for small nanoparticles.

The Controlled Synthesis of Delafossite $CuGaO_2$ Nanoparticles and Nanoplates. On the basis of the discussion above, the OA growth should be suppressed by maximizing the electrostatic and steric repulsions to obtain small $CuGaO_2$ nanoparticles. Therefore, the optimum synthetic conditions should be a precursor pH far from the $CuGaO_2$ IEP, a high reaction temperature, the addition of appropriate surfactants, a low precursor concentration, and a short reaction time. Experimentally, we optimized the conditions as 0.15 mmol of $Cu(NO_3)_2$, $Ga(NO_3)_3$, and SDS dissolved in deionized water with the pH tuned to ∼2.8 by the addition of KOH solution. The total volume was kept at 13 mL with another 1 mL of ethylene glycol added. The overnight-stirred precursor was then sealed in a 23 mL Teflon-lined autoclave to

dx.doi.org/10.1021/ic500747x | Inorg. Chem. 2014, 53, 5845−5851

Scheme 2. The Proposed OA Growth Process of the Delafossite $CuGaO_2$ Nanocrystals

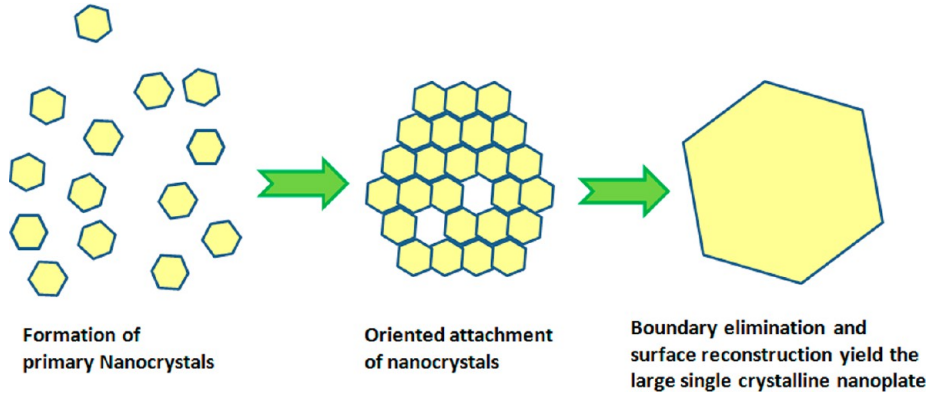

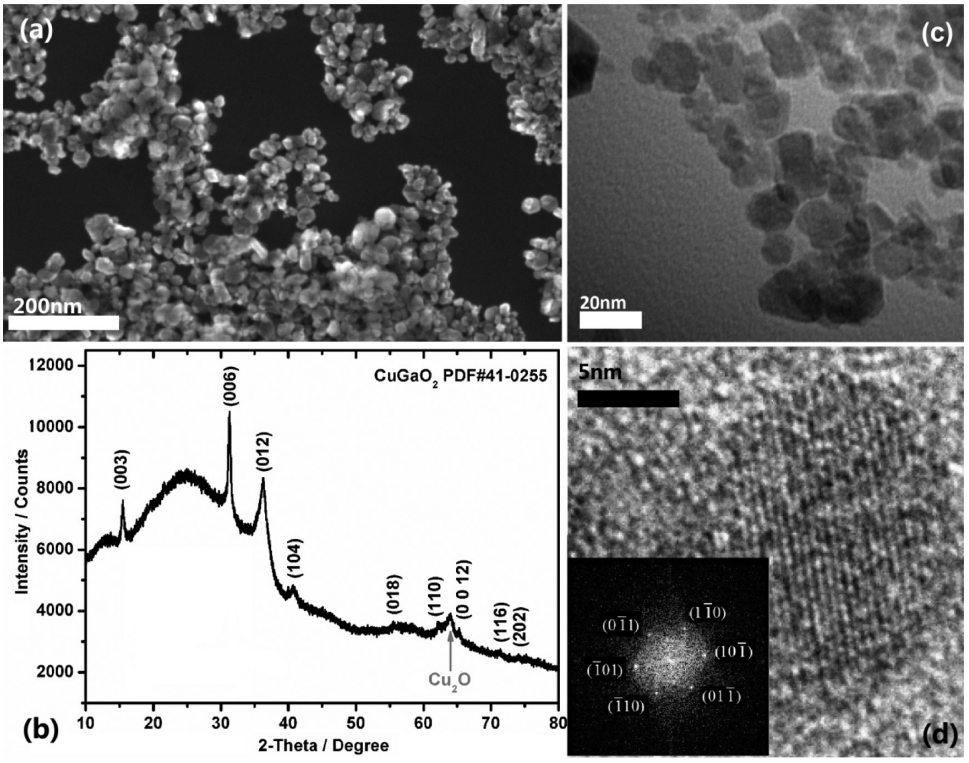

Figure 6. Characterizations of the delafossite $CuGaO_2$ nanoparticles. (a) The SEM image. (b) The XRD pattern. (c) The TEM image. (d) The HRTEM image. (inset) The fast Fourier transform (FFT) pattern from the selected area.

undergo a hydrothermal reaction at 240 °C for 4 h. After the reaction, the upper suspension layer was separated, and the white-colored nanoparticles were collected. Excitingly, the SEM, TEM, and XRD results (Figure 6, Supporting Information, Figure S4) clearly show that the 3*R* delafossite phase $CuGaO_2$ nanocrystals with sizes of ∼20 nm were successfully synthesized. According to the XRD, the average crystalline size is calculated to be 21 nm based on the Scherrer equation, indicating these nanoparticles are single crystalline. This is the first time that 20 nm delafossite $CuGaO_2$ nanocrystals have been synthesized, with only a little Cu_2O impurity detected, which can be removed by washing with a dilute ammonia solution.

On the other hand, synthesis of large $CuGaO_2$ nanoplates can be achieved by promoting OA growth. Reaction conditions with a solution pH close to the $CuGaO_2$ IEP, a low reaction temperature, a long reaction time, a high concentration of the precursor, and the absence of surfactants are preferred. For example, an excellent synthetic procedure for synthesizing micrometer-sized delafossite $CuGaO_2$ nanoplates is 0.48 mmol of $Cu(NO_3)_2$ and $Ga(NO_3)_3$ dissolved in deionized water with the pH at ∼7 tuned by the addition of KOH solution. The total volume was kept at 14 mL with 2 mL of ethylene glycol added. The overnight-stirred precursor was then sealed in a 23 mL Teflon-lined autoclave to undergo a hydrothermal reaction at 190 °C for 52 h. After the reaction, the gray-colored product was collected. SEM, TEM, and XRD show the product contains phase-pure single crystalline delafossite $CuGaO_2$ nanoplates with the diameter on a micrometer scale and the thickness of ∼100 nm. (Figure 7) The XRD pattern shows that the (0 0 *l*) diffraction peak family (based on hexagonal 2*H* indexes) is much more intense than the others, indicating the preferred orientation of these particles, which is in consistent with their platelike morphology.

dx.doi.org/10.1021/ic500747x | *Inorg. Chem.* 2014, 53, 5845−5851

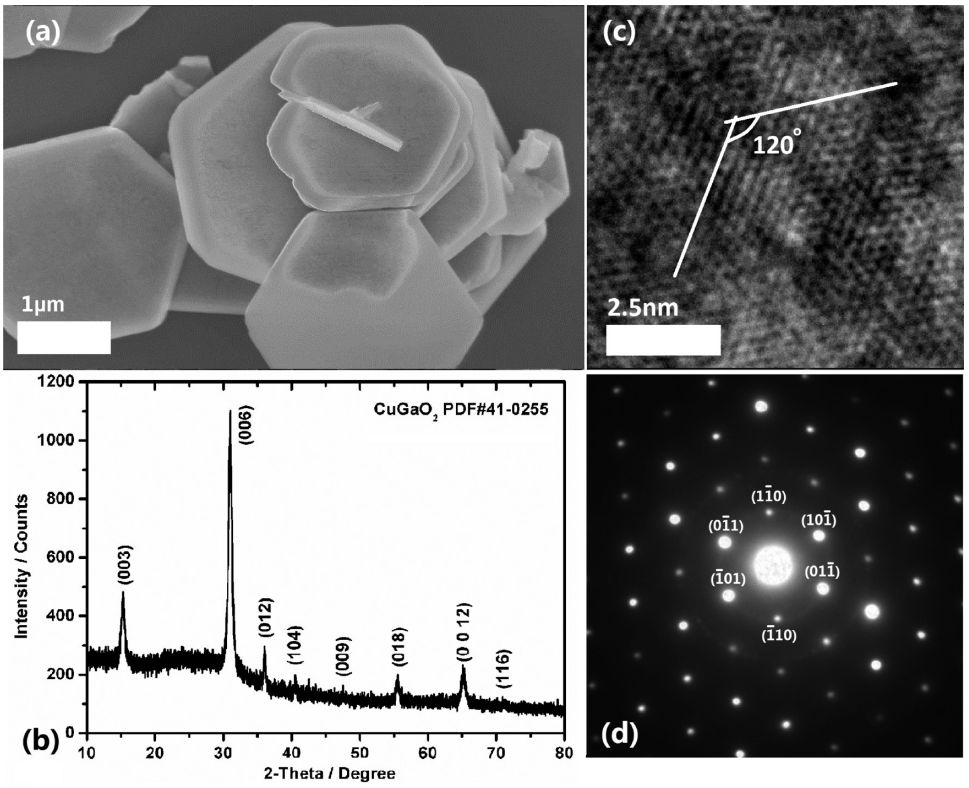

Figure 7. Characterizations of the large delafossite $CuGaO_2$ nanoplates. (a) The SEM image. (b) The XRD pattern. (c) The HRTEM image. (d) the selected-area electron diffraction (SAED) pattern.

CONCLUSION

To summarize, we systematically studied the phase formation and the crystal growth mechanism of the delafossite $CuGaO_2$ under low-temperature hydrothermal conditions. By performing the reaction with a temperature higher than 180 °C and a precursor pH within the range from ~3.4 to ~6.6, the stabilization of $Cu^{+}_{[aq]}$ and the control of the hydrolyzed $[Ga(OH)_3(H_2O)_3]^0$ and $[Ga(OH)_4(H_2O)]^-$ species can be achieved, and therefore the delafossite $CuGaO_2$ phase is formed. The OA growth process is proposed as the growth mechanism for large $CuGaO_2$ nanoplates: primary $CuGaO_2$ nanocrystals are first formed and then go through the OA growth process, forming large nanoplates. By promoting or suppressing this process, both small nanoparticles (~20 nm) and large nanoplates (>1 μm in diameter) were selectively synthesized. This is the first report of 20 nm delafossite $CuGaO_2$ nanocrystal synthesis. Moreover, considering the structural and chemical similarities of the copper-based delafossite compounds, the understanding of the hydrothermal chemistry and crystallization mechanism of delafossite $CuGaO_2$ should also benefit syntheses of other similar compounds, such as $CuAlO_2$ and $CuScO_2$.

EXPERIMENTAL SECTION

All chemicals were used as received: gallium nitrate hydrate (99.9%), copper nitrate hemi(pentahydrate) (98.0−102.0%), and potassium hydroxide from Alfa Aesar; ethylene glycol (>99%) and sodium dodecyl sulfate (SDS, 99%) from Sigma-Aldrich; 200 proof ethyl alcohol, ACS-grade isopropyl alcohol and methanol from Fisher Scientific; and deionized water (resistivity =18 MΩ cm) from the Barnstead E-Pure system. The Teflon-lined 23 mL autoclaves from the Parr company were used in the syntheses. The pH of the precursor was measured by the Oakton Ion6 pH/Ion/°C-Meter from the Oakton Instruments. The synthesized products were characterized by powder X-ray diffraction (XRD, Cu Kα, Rigaku Inc.), scanning electron microscopy (SEM, Sirion, FEI Company), and transmission electron microscopy (TEM, the CM-200T, and the Probe Corrected Titan380−300 S/TEM for high-resolution TEM (HRTEM), FEI company). The zeta potential was measured by the ZETASIZER Nano-ZS from Malvern Instruments.

The Temperature-Variable Syntheses. 0.48 mmol of $Cu(NO_3)_2$ and $Ga(NO_3)_3$ was dissolved in deionized water with the pH tuned to 5.5 by the addition of KOH solution. The final volume of the precursor was kept at 12 mL with 2 mL of ethylene glycol added. The overnight-stirred precursor was then sealed in a 23 mL Teflon-lined autoclave to undergo a hydrothermal reaction at the designated temperature (170 to 240 °C) for 48 h in a preheated oven. After the reaction, the particles were collected by centrifuging and were washed with ethanol and water several times for characterizations.

The pH-Variable Syntheses. 0.48 mmol of $Cu(NO_3)_2$ and $Ga(NO_3)_3$ was dissolved in deionized water with the pH tuned by the addition of KOH solution. The final volume of the precursor was kept at 12 mL. Since the K_w of water changes from 10^{-14} at 25 °C to ~10^{-12} at 190 °C, the reported pH values of the precursors at 190 °C were calculated from its measured pH value at room temperature. All the following procedures were kept the same as in the Temperature-Variable Syntheses section except the reaction temperature, which was set to 190 °C for all trials.

The Syntheses with γ-GaO(OH) as the Precursor. The γ-GaO(OH) powder was synthesized by hydrothermally heating the $Ga(OH)_3$ colloid (pH ≈ 3.5) at 190 °C for 10 h. After being washed and dried in a vacuum desiccator, the white γ-GaO(OH) powder was obtained. Then 0.48 mmol of γ-GaO(OH) powder was used in the precursor to replace the gallium nitrate for the synthesis. All the following procedures were kept the same as in the Temperature-Variable Syntheses section except the reaction temperature, which was set to 190 °C.

Monitoring the Intermediate Products during the Hydrothermal Reaction Process. 0.48 mmol of $Cu(NO_3)_2$ and $Ga(NO_3)_3$

dx.doi.org/10.1021/ic500747x | Inorg. Chem. 2014, 53, 5845−5851

was dissolved in deionized water with the pH tuned to 5.5 by the addition of KOH solution. The final volume of the precursor was 12 mL with 2 mL of ethylene glycol added. The overnight-stirred precursor was then sealed in a 23 mL Teflon-lined autoclave to undergo a hydrothermal reaction at 190 °C in a preheated oven. The reaction was stopped by taking the autoclave out of the oven at different reaction times (e.g., 6 h, 12 h, 18 h, etc.) and quenching under flowing water. The intermediate product was collected by centrifuging and was washed with ethanol and water several times before characterizations.

■ ASSOCIATED CONTENT

Ⓢ Supporting Information

This includes the XRD results for $CuGaO_2$ synthesis with different reducing reagents, zeta potential measurement of $CuGaO_2$, SEM images with different amounts of surfactant added in the precursor, SEM images of $CuGaO_2$ nanoparticles on a larger scale, Pourbaix diagrams for copper, and distribution of Ga^{III} aqueous species as a function of pH at different temperatures. This material is available free of charge via the Internet at http://pubs.acs.org.

■ AUTHOR INFORMATION

Corresponding Author

*E-mail: wu@chemistry.ohio-state.edu. Phone: (+1)614-247-7810. Fax: (+1) 614-292-1685.

Notes

The authors declare no competing financial interest.

■ ACKNOWLEDGMENTS

The authors acknowledge the support from the United States Department of Energy (Award No. DE-FG02-07ER46427). Dr. D. Bong and Z. Zhou are acknowledged for assistance in the collection of the Zeta potential data. H. Colijn and the Ohio State University Center for Electron Microscopy and Analysis (CEMAS) are acknowledged for assistance in the collection of HRTEM images.

■ REFERENCES

(1) Yanagi, H.; Kawazoe, H.; Kudo, A.; Yasukawa, M.; Hosono, H. *J. Electroceram.* **2000**, *4*, 407−414.
(2) Sheng, S.; Fang, G.; Li, C.; Xu, S.; Zhao, X. *Phys. Status Solidi A* **2006**, *203*, 1891−1900.
(3) Nie, X.; Wei, S.-H.; Zhang, S. B. *Phys. Rev. Lett.* **2002**, *88*, 066405.
(4) Fang, Z.-J.; Fang, C.; Shi, L.-J.; Liu, Y.-H.; He, M.-C. *Chin. Phys. Lett.* **2008**, *25*, 2997.
(5) Gillen, R.; Robertson, J. *Phys. Rev. B* **2011**, *84*, 035125.
(6) Benko, F. A.; Koffyberg, F. P. *Phys. Status Solidi A* **1986**, *94*, 231−234.
(7) Ueda, K.; Hase, T.; Yanagi, H.; Kawazoe, H.; Hosono, H.; Ohta, H.; Orita, M.; Hirano, M. *J. Appl. Phys.* **2001**, *89*, 1790−1793.
(8) Gurunathan, K.; Baeg, J.-O.; Lee, S. M.; Subramanian, E.; Moon, S.-J.; Kong, K.-J. *Catal. Commun.* **2008**, *9*, 395−402.
(9) Kato, S.; Fujimaki, R.; Ogasawara, M.; Wakabayashi, T.; Nakahara, Y.; Nakata, S. *Appl. Catal., B* **2009**, *89*, 183−188.
(10) Lekse, J. W.; Underwood, M. K.; Lewis, J. P.; Matranga, C. *J. Phys. Chem. C* **2011**, *116*, 1865−1872.
(11) Renaud, A.; Chavillon, B.; Le Pleux, L.; Pellegrin, Y.; Blart, E.; Boujtita, M.; Pauporte, T.; Cario, L.; Jobic, S.; Odobel, F. *J. Mater. Chem.* **2012**, *22*, 14353−14356.
(12) Yu, M.; Natu, G.; Ji, Z.; Wu, Y. *J. Phys. Chem. Lett.* **2012**, *3*, 1074−1078.
(13) Alias, A.; Mohamad, K. A.; Gosh, B. K.; Sakamoto, M.; Uesugi, K. *ICSE 2012, IEEE Int. Conf. Semicond. Electron., Proc.* **2012**, 763−765.
(14) Yu, M.; Draskovic, T. I.; Wu, Y. *Phys. Chem. Chem. Phys.* **2014**, *16*, 5026−5033.
(15) Renaud, A.; Cario, L.; Deniard, P.; Gautron, E.; Rocquefelte, X.; Pellegrin, Y.; Blart, E.; Odobel, F.; Jobic, S. *J. Phys. Chem. C* **2014**, *118*, 54−59.
(16) Forticaux, A.; Hacialioglu, S.; DeGrave, J. P.; Dziedzic, R.; Jin, S. *ACS Nano* **2013**, *7*, 8224−8232.
(17) Xu, Z.; Xiong, D.; Wang, H.; Zhang, W.; Zeng, X.; Ming, L.; Chen, W.; Xu, X.; Cui, J.; Wang, M. *J. Mater. Chem. A* **2014**, *2*, 2968−2976.
(18) Park, S.; Keszler, D. A. *J. Solid State Chem.* **2003**, *173*, 355−358.
(19) Gall, R. B.; Ashmore, N.; Marquardt, M. A.; Tan, X.; Cann, D. P. *J. Alloys Compd.* **2005**, *391*, 262−266.
(20) Han, M. J.; Jiang, K.; Zhang, J. Z.; Li, Y. W.; Hu, Z. G.; Chu, J. H. *Appl. Phys. Lett.* **2011**, *99*, 131104−131103.
(21) Varadarajan, V.; Norton, D. P. *Appl. Phys. A: Mater. Sci. Process.* **2006**, *85*, 117−120.
(22) Kumar, S.; Miclau, M.; Martin, C. *Chem. Mater.* **2013**, *25*, 2083−2088.
(23) Srinivasan, R.; Chavillon, B.; Doussier-Brochard, C.; Cario, L.; Paris, M.; Gautron, E.; Deniard, P.; Odobel, F.; Jobic, S. *J. Mater. Chem.* **2008**, *18*, 5647−5653.
(24) Sheets, W. C.; Mugnier, E.; Barnabé, A.; Marks, T. J.; Poeppelmeier, K. R. *Chem. Mater.* **2005**, *18*, 7−20.
(25) Shahriari, D. Y.; Barnabe, A.; Mason, T. O.; Poeppelmeier, K. R. *Inorg. Chem.* **2001**, *40*, 5734−5735.
(26) Chavillon, B.; Cario, L.; Doussier-Brochard, C.; Srinivasan, R.; Le Pleux, L.; Pellegrin, Y.; Blart, E.; Odobel, F.; Jobic, S. *Phys. Status Solidi A* **2010**, *207*, 1642−1646.
(27) Beverskog, B.; Puigdomenech, I. *J. Electrochem. Soc.* **1997**, *144*, 3476−3483.
(28) Baes, C. F.; Mesmer, R. E. *The Hydrolysis of Cations;* Wiley: New York, 1976; Vol. *68*.
(29) Benézéth, P.; Diakonov, I. I.; Pokrovski, G. S.; Dandurand, J.-L.; Schott, J.; Khodakovsky, I. L. *Geochim. Cosmochim. Acta* **1997**, *61*, 1345−1357.
(30) Laubengayer, A.; Engle, H. *J. Am. Chem. Soc.* **1939**, *61*, 1210−1214.
(31) Bonet, F.; Tekaia-Elhsissen, K.; Sarathy, K. V. *Bull. Mater. Sci.* **2000**, *23*, 165−168.
(32) Voorhees, P. W. *J. Stat. Phys.* **1985**, *38*, 231−252.
(33) Penn, R. L.; Banfield, J. F. *Science* **1998**, *281*, 969−971.
(34) Wang, F.; Richards, V. N.; Shields, S. P.; Buhro, W. E. *Chem. Mater.* **2014**, *26*, 5−21.
(35) Penn, R. L.; Banfield, J. F. *Am. Mineral.* **1998**, *83*, 1077−1082.
(36) Banfield, J. F.; Welch, S. A.; Zhang, H.; Ebert, T. T.; Penn, R. L. *Science* **2000**, *289*, 751−754.
(37) Zhang, Q.; Liu, S.-J.; Yu, S.-H. *J. Mater. Chem.* **2009**, *19*, 191−207.
(38) Lee, E. J. H.; Ribeiro, C.; Longo, E.; Leite, E. R. *J. Phys. Chem. B* **2005**, *109*, 20842−20846.
(39) Li, D.; Nielsen, M. H.; Lee, J. R. I.; Frandsen, C.; Banfield, J. F.; De Yoreo, J. J. *Science* **2012**, *336*, 1014−1018.
(40) Rabenau, A. *Angew. Chem., Int. Ed. Engl.* **1985**, *24*, 1026−1040.